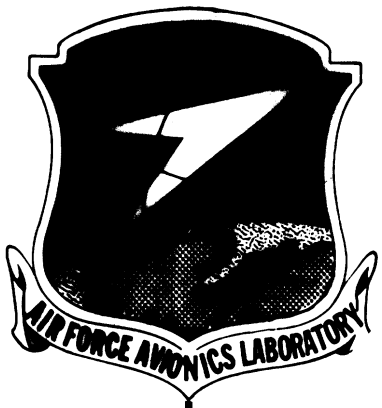

Air Force Avionics Laboratory
Research and Technology Division
Air Force Systems Command
Wright-Patterson Air Force Base, Ohio

TRANSMITTER IMPEDANCE CHARACTERISTICS FOR AIRBORNE SPECTRUM SIGNATURE

Interim Technical Report No. 5
1 April - 30 June 1967

J. E. Ferris, W. R. DeHart and W. B. Henry

15 July 1967

Contract AF-33(615)-3454

Contract Monitor: K. W. Tomlinson AVWE

7956-5-T = RL-2170

THE UNIVERSITY OF MICHIGAN
COLLEGE OF ENGINEERING
DEPARTMENT OF ELECTRICAL ENGINEERING
Radiation Laboratory

Administered through:
OFFICE OF RESEARCH ADMINISTRATION • ANN ARBOR

TABLE OF CONTENTS

ABSTRACT

A more general method for making source impedance measurements has been investigated during this reporting period. Previous methods for determining the impedance of a transmitter required varying the phase angle of the load impedance by at least 90 electrical degrees. Employing this more general technique, it is necessary to change the phase of the impedance a few degrees only; after performing an analysis of the data, one can then determine the transmitter impedance. In addition to this technique, an analytical analysis of a class C amplifier has been performed to determine the spectrum signature of such an amplifier. Included in this report is a discussion of the construction of the class C amplifier and its theory of operation. A third aspect of the program during this reporting period has been the collection of additional harmonic Rieke diagrams for an ARC-27 and ARC-34 transmitter.

I. INTRODUCTION

The statement of problem as set forth in the contract which provides for the present investigation is as follows:

1) A determination of the power delivered to the antenna for "spectrum signature" purposes will require a measurement of the antenna impedance, transmission line characteristics, transmitter maximum power output, and transmitter output impedance at the fundamental, spurious and harmonic frequencies. The transmitter output impedance at the spurious and harmonic frequencies is not well understood and therefore, requires further study. The prime payoff in this study will be better "spectrum signatures" for more accurate predictions of interference between systems.

2) There is a requirement to verify the results of the earlier successful program, Contract AF 33(615)-2606 "Simplified Modeling Techniques for Avionic Antenna Pattern Signatures", with a mock-up of an aircraft transmitter system.

3) The stated objective of the contract is: To conclude the development of "simplified" techniques for determining the RF spectrum signatures of flight vehicle electronics systems. To establish the validity of the techniques by comparing the results of data obtained by the "simplified" techniques with data obtained from tests employing a typical transmitter system in a mock-up.

4) The present phase of the contract is concerned with developing a technique for the accurate prediction of the power output of a typical transmitter. The realization of such a technique requires a thorough knowledge of a transmitter's output as a function of the parameters most likely to vary in a practical situation at not only the fundamental frequency but the harmonic and spurious frequencies as well.

II. SOURCE IMPEDANCE MEASUREMENT

Techniques for measuring the impedance of a source (i.e., a transmitter) have been discussed in previous interim reports. This discussion presents a more general method for making such measurements. The two previously proposed measurement schemes are specific applications of this more general technique.

The methods previously described for determining the impedance of a transmitter included varying the phase angle of the load impedance by at least 90 electrical degrees. This technique, while adequate for laboratory measurements on transmitters whose parameters do not vary as a function of the load impedance, is unsatisfactory for a wide range of sources. The basis for a scheme which minimizes the change of load impedance necessary for transmitter impedance measurements is described below.

One concept for measuring the transmitter impedance is shown schematically in Fig. 2-1.

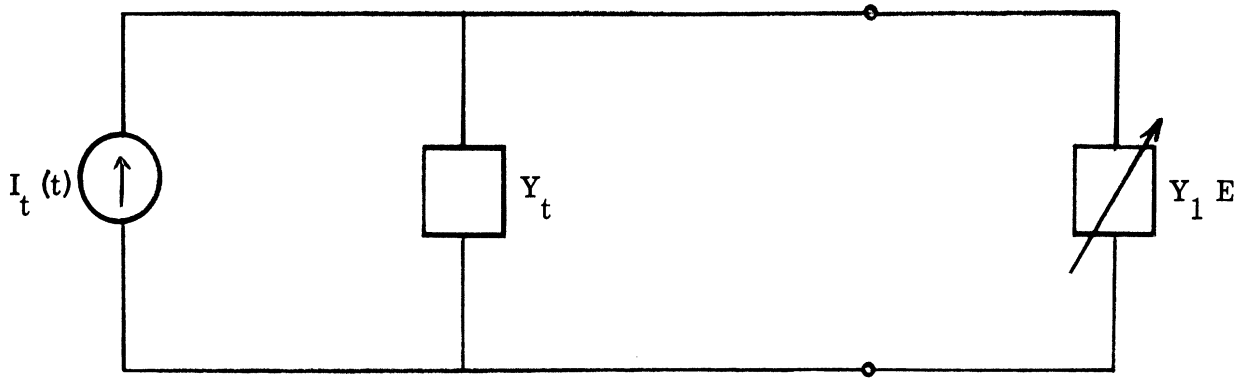

FIG. 2-1: Transmitter Equivalent Circuit and Variable Load

The transmitter is modeled by its equivalent current source $I_t = |I_t| \sin \omega t$, and internal admittance Y_t; the load is Y_ℓ. The voltage E is measured for two values of Y_ℓ, Y_1 and Y_2. The following equations apply.

$$I_t = E_1 (Y_t + Y_1) \tag{2.1}$$

$$I_t = E_2 (Y_t + Y_2) \tag{2.2}$$

Combining equations (2.1) and (2.2),

$$E_1 (Y_t + Y_1) = E_2 (Y_t + Y_2) \tag{2.3}$$

From which,

$$Y_t = \frac{E_1 Y_1 - E_2 Y_2}{E_2 - E_1} = \frac{Y_1 - \frac{E_2}{E_1} Y_2}{\frac{E_2}{E_1} - 1} \tag{2.4a,b}$$

It must be remembered that Y_t, Y_1, Y_2, E_1, and E_2 are in general complex quantitives, hence

$$Y_t = G_t + j B_t \tag{2.5a}$$

$$Y_1 = G_1 + j B_1 \tag{2.5b}$$

$$Y_2 = G_2 + j B_2 \tag{2.5c}$$

$$E_1 = |E_1| e^{j\theta_1} \tag{2.5d}$$

$$E_2 = |E_2| e^{j\theta_2} \tag{2.5e}$$

The ratio E_2/E_1 becomes,

$$\frac{E_2}{E_1} = \left|\frac{E_2}{E_1}\right| \frac{e^{j\theta_2}}{e^{j\theta_1}} = \left|\frac{E_2}{E_1}\right| e^{j(\theta_2 - \theta_1)} \tag{2.6a}$$

$$\left|\frac{E_2}{E_1}\right| \left[\cos(\theta_2 - \theta_1) + j \sin(\theta_2 - \theta_1)\right] \tag{2.6b}$$

Substituting equations (2.5a, b, c) and (2.6b) into (2.4) and setting $\left|\frac{E_2}{E_1}\right| \cos(\theta_2 - \theta_1) = a$; $\left|\frac{E_2}{E_1}\right| \sin(\theta_2 - \theta_1) = b$ for convenience we continue

$$G_t + jB_t = \frac{G_1 + jB_1 - (a + jb)(G_2 + jB_2)}{(a + jb) - 1} \tag{2.7}$$

Separating the real and imaginary components of (2.7),

$$G_t = \frac{G_1(a - 1) + B_1(b) + G_2(-a^2 + a - b^2) + B_2(-b)}{(a - 1)^2 + b^2} \tag{2.8a}$$

$$B_t = \frac{G_1(-b) + B_1(a - 1) + G_2(b) + B_2(-a^2 + a - b^2)}{(a - 1)^2 + b^2} \tag{2.8b}$$

Equations (2.8a, b) and Fig. 2-1 describe a very general method for determining a transmitter's output admittance. One specific variation of Fig 2-1 is shown in Fig. 2-2. It is interesting to note parenthetically that the methods previously

described for determining the transmitter impedance are simply special cases of (2.8a,b) where $(\theta_2 - \theta_1) = \frac{\pi}{2}$ and Z_1 is transformed to the point where $Z_t' = R_t'$ implying that $Y_t' = G_t'$.

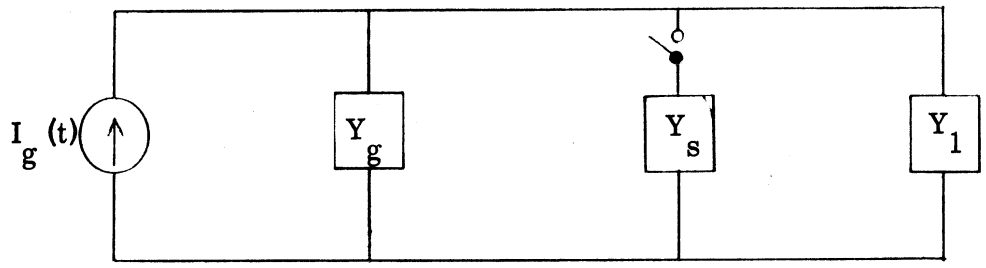

FIG. 2-2: A Variable Load Method for Transmitter Impedance Measurement

In Fig. 2-2, Y_s is a small admittance which can be switched into the circuit. Thus Y_1 and Y_2 (equations (2.4a,b) would become Y_1 and $Y_1 + Y_s$ respectively. In practice, when dealing with a transmitter whose output parameters vary with load admittance, one could choose Y_1 equal to the actual load admittance which would be placed on the transmitter terminals in actual service. Y_s could then be chosen sufficiently small (commensurate with measurement equipment accuracy) to effectively preclude variations of the transmitter parameters.

III. SPECTRUM SIGNATURE ANALYSIS OF A CLASS C AMPLIFIER

Much work has been done in the past few months to develop methods for determining the spectrum signature of a transmitter. The analysis at present includes an assumption that the transmitter output voltage varies linearly with the load impedance at each frequency for which there is an output present. The output of such a linear device may then be calculated as a function of load impedance once, a) the device internal impedance, and b) power output into a known load have been determined at each frequency of interest. Large deviations in power output and degree of linearity are experienced from unit to unit, necessitating a complete series of measurements for each transmitter and load in question. This is obviously a very time consuming procedure. The purpose of this study is to determine feasible methods to calculate the spectrum signature of that class of transmitters as a function of the tube bias and load conditions. The transmitters to be considered utilize a cw or plate modulated vacuum tube class C final amplifying stage. The experiment includes developing a model for predicting the spectrum signature of a class C amplifier and comparing these results with the actual output of a laboratory amplifier, designed and constructed especially for this purpose.

3.1 Theoretical Analysis

This section will be concerned with developing a large signal model of a vacuum tube and calculating the Fourier components of the model output (the notation used is standard as listed in the Appendix). The classical model is discussed

along with a modified version designed to yield more accurate results.

3.2 The Classical Model

The classical approach to class C amplifier spectrum signature analysis includes modeling the tube and its output circuitry by a current source and shunt admittance (Cheng, 1959) as shown in Fig. 3-1. For this type of analysis, it is usually assumed that the plate current is a linear function of the grid voltage for those values of grid voltage above the tube cut-off value.

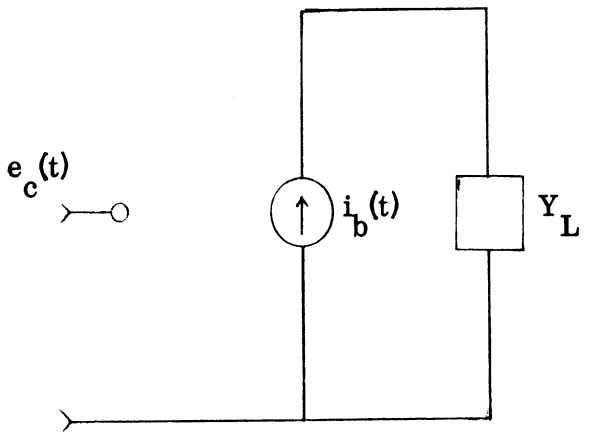

FIG. 3-1: Classical Model: $i_b(t) = K_1 e_c(t) + K_2$

$$i_b = K_1 e_c + K_2 \quad \text{for } e_c \geq e_{co} \tag{3.1}$$

$$i_b = 0 \quad \text{for } e_c < e_{co}$$

where e_{co} is the greatest value of control grid voltage for which no plate current flows. From (3.1), it is evident that if the grid voltage is a sinusoid of agrument

ωt, the plate voltage will be a truncated and rectified sinusoid of the same argument. Let

$$e_c = \left|\hat{E}_g\right|_1 \sin \omega t + E_{cc} \tag{3.2}$$

then

$$i_b = K_1 \left(\left|\hat{E}_g\right|_1 \sin \omega t + E_{cc} \right) + K_2$$

$$\text{for} \left(\left|\hat{E}_g\right|_1 \sin \omega t + E_{cc} \right) \geq e_{co} \tag{3.3}$$

$$i_b = 0$$

$$\text{for } \left|\hat{E}_g\right|_1 \sin \omega t + E_{cc} < e_{co}.$$

Once K_1 is specified, the Fourier components of i_b can be calculated.

$$i_b = \bar{I}_b + \sum_n \left|\hat{I}_p\right|_n \sin (n \omega t + \phi_n)$$

$$= 1/2\, A_o + \sum_n A_n \cos n \omega t + b_n \sin n \omega t \tag{3.4}$$

where

$$A_n = \frac{1}{\pi} \int_0^{2\pi} i_b (t) \cos_n \omega t \, d\omega t$$

$$b_n = \frac{1}{\pi} \int_0^{\pi} i_b (t) \sin_n \omega t \, d\omega t \tag{3.5}$$

The power output of the device is given by

$$P_{out} = \sum_n P_n = \frac{1}{2} \sum_n |I_p|_n^2 R_e [Z_n] \qquad (3.6)$$

where $R_e [Z_n]$ is the real part of the load impedance at the angular frequency $(n\omega)$.

3.3 An Improved Model

The approximation for i_b given by (3.3), while sufficient for many applications, is not difficult to improve. Figure 3-2 is the static characteristic curves of a dual tetrode (Amperex 6252). In the classical approach just discussed, it describes constant current curves which are linearly spaced, horizontal straight lines. It is evident from these characteristics that the constant current contours are not horizontal, especially for low values of plate voltage and are not linearly spaced. (The constant current contours of a triode have in fact a much steeper slope than those in Fig. 3-2). To account for the non-zero slope and slope variations with plate voltage, the curves can be accurately represented by piece-wise linear approximations as given by (3.7) (see Fig. 3-3).

$$i_b = A_r e_c + B_s e_b + C_r \quad \text{for } e_{c(r-1)} > e_c \geq e_{c(r)}$$

$$\text{and } e_{b(s-1)} > e_b > e_{b(s)} \qquad (3.7)$$

$$i_b = 0 \quad e_c \leq e_{co}$$

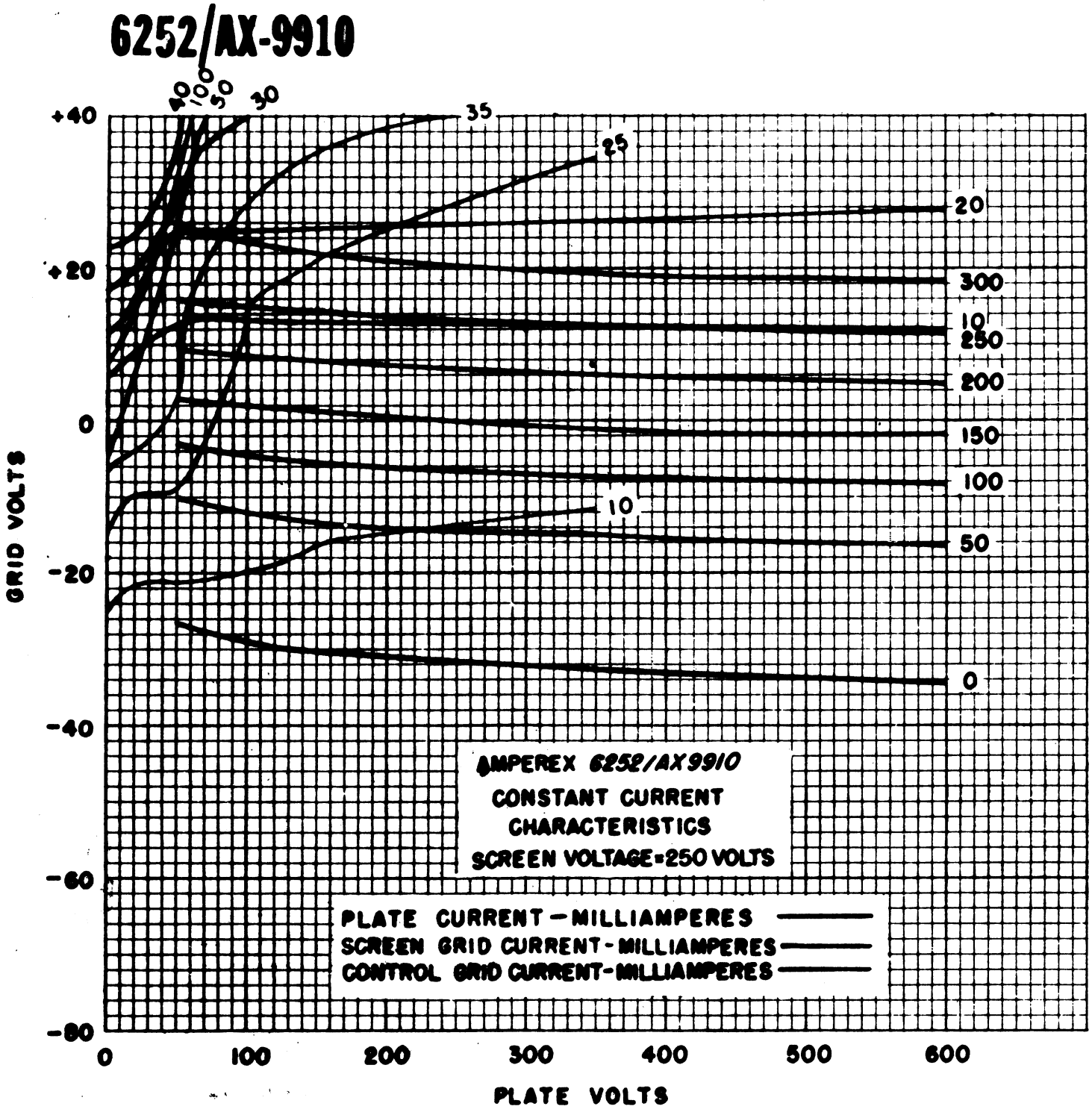

FIG. 3-2: Static Characteristic Curves for 6252

where A_r, B_s, and C_r are appropriately chosen constants over the region $e_{c\,(r-1)}$ to $e_{c(r)}$ and $e_{b\,(s-1)}$ to $e_{b(s)}$. In general, any desired accuracy can be attained simply by increasing the number of piece-wise linear approximations of the form (3.7) to the experimental characteristics.

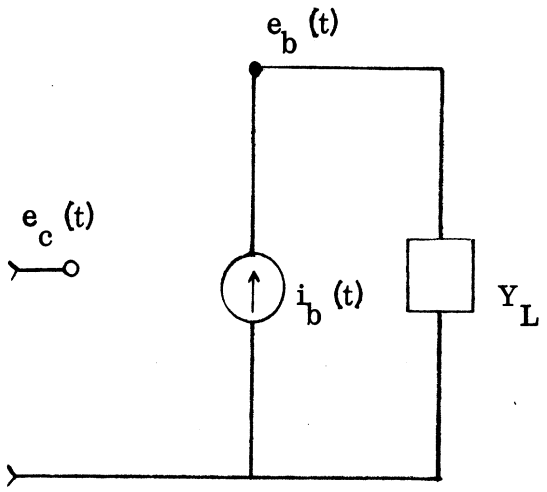

FIG. 3-3: Improved Model: $i_b(t) = A_r e_c(t) + B_s e_b(t) + e_r$

Including the second variable, e_b, in the equation for i_b (3.7) has, however, introduced some additional complications. Consider (3.7) together with the constant,

$$\left|\hat{E}_{p\,n}\right| = \left|\hat{I}_{p\,n}\right| Z_n \qquad (3.8)$$

Moving the dependent variable e_b to the left hand side of the equation and solving for i_b,

$$i_b - B_s e_b = I_b (1-B_s) + \sum_{n=1}^{\infty} \left|\hat{I}_p\right|_n \sin (n\omega t + \phi_n) \cdot (1 - B_s Z_n) = A_r e_c + C_r \qquad (3.9)$$

for $e_c > e_{co}$

where

$$Z_n = Z_n (jr\omega) = \left|Z_n\right| \left[\cos \gamma_n + j \sin \gamma_n\right] \qquad (3.10)$$

A casual inspection suggests setting $e_c = E_g, \sin \omega t + E_{cc}$ as in (3.2) and integrating over the period $\omega t = 2\pi$ to obtain an expression relating the constant terms on each side of (3.9). It must be noted, however, that (3.9) is valid only for $e_c \geq e_{co}$ prohibiting this approach. Assuming that e_c is of the form (3.2) or any other completely specified form) we are able to solve (3.9) for i_b (t) by a series of successive approximations. The method is as follows:

1) Assume $e_c = E_{cc} - \left|\hat{E}_g\right|, \sin \omega t$ and $e_b = E_{bb} - \left|\hat{E}_b\right|, \cos \omega t$ (this is equivalent to stipulating $Z_1 = R_1, \; Z_n = 0 \; n \neq 1$).

2) Calculate i_b (b) from (3.7).

3) Determine the Fourier components of i_b.

4) Solve $e_b(t) = \bar{I}_o R_o + \sum_{n=1}^{\infty} \left|\hat{I}_p\right|_n \sin (n\omega t + \phi_n). \; Z_n$ where Z_n is given by 10.

5) Substitute this expression for e_b (t) into (3.7) and calculate a new value of i_b(t).

6) Repeat the sequence 2) - 5) until i_b(t) has been obtained to the desired accuracy.

The power output as a function of frequency is then the same as given by (3.6). Clearly this type of solution requires many calculations for each new set of parameters that are investigated. However, it lends itself well to techniques utilizing a digital computer.

3.4 A Comparison of the Models

To evaluate the improvement afforded by the piece-wise linear model described above, an input (e_c) and plate load impedance were selected for the tube and the resulting first three Fourier components of the plate current waveform calculated from: 1) the actual tube characteristics, 2) the classical model, 3) a four-region piece-wise linear model, and 4) a six-region piece-wise linear model. The procedure was as follows. Assuming the grid and plate voltages to be sinusoids of period ωt and 180^o out of phase

$$e_c = E_{cc} + \left|\hat{E}_g\right|, \sin \omega t$$

$$e_b = E_{bb} + \left|\hat{E}_p\right|, \cos \omega t \qquad (3.11)$$

a value of plate current is specified for each value of ωt. These values were tabulated and plotted for $-\frac{\pi}{2} \leq \omega t \leq \frac{\pi}{2}$. The Fourier components are then given by (3.4) and (3.5). In order to evaluate the coefficients A_n and b_n, it is necessary only to plot $i_b(t) \cos(\omega nt)$, $i_b(t) \sin(\omega nt)$. The integral of $i_b(t) \cos(\omega nt)$ is then the area under the curve grounded by the ωt axis, (Skilling, 1957). For this example, the symmetries present (even function and quarter wave symmetry) assuming a symmetric dual tube (see Fig. 3-4), require only odd harmonics of even functions. The curves appear in Figs. 3-5 through 3-8, the model in Table 3-1, and the results in Table 3-2. Notice that the results of the third model represent about a 10 per cent improvement over the classical model.

3.5 Amplifier Design and Construction

Since the purpose of the experiment is to determine the spectrum signature of a class C amplifier as a function of its operating characteristics, it is imperative that the design be kept as flexible as possible to allow the desired changes to be readily made. The first part of this section discusses the general problem of the design of a class C amplifer, and the second details of the procedure followed for the unit which has been constructed. Finally, the third portion deals with the hardware realizations of the required circuit elements and describes the completed unit.

3.6 Design of a Class C Amplifier

A class C amplifier is an amplifier for which the grid bias is so large that plate current flows for less than one half the cycle. A sketch of i_b versus e_c

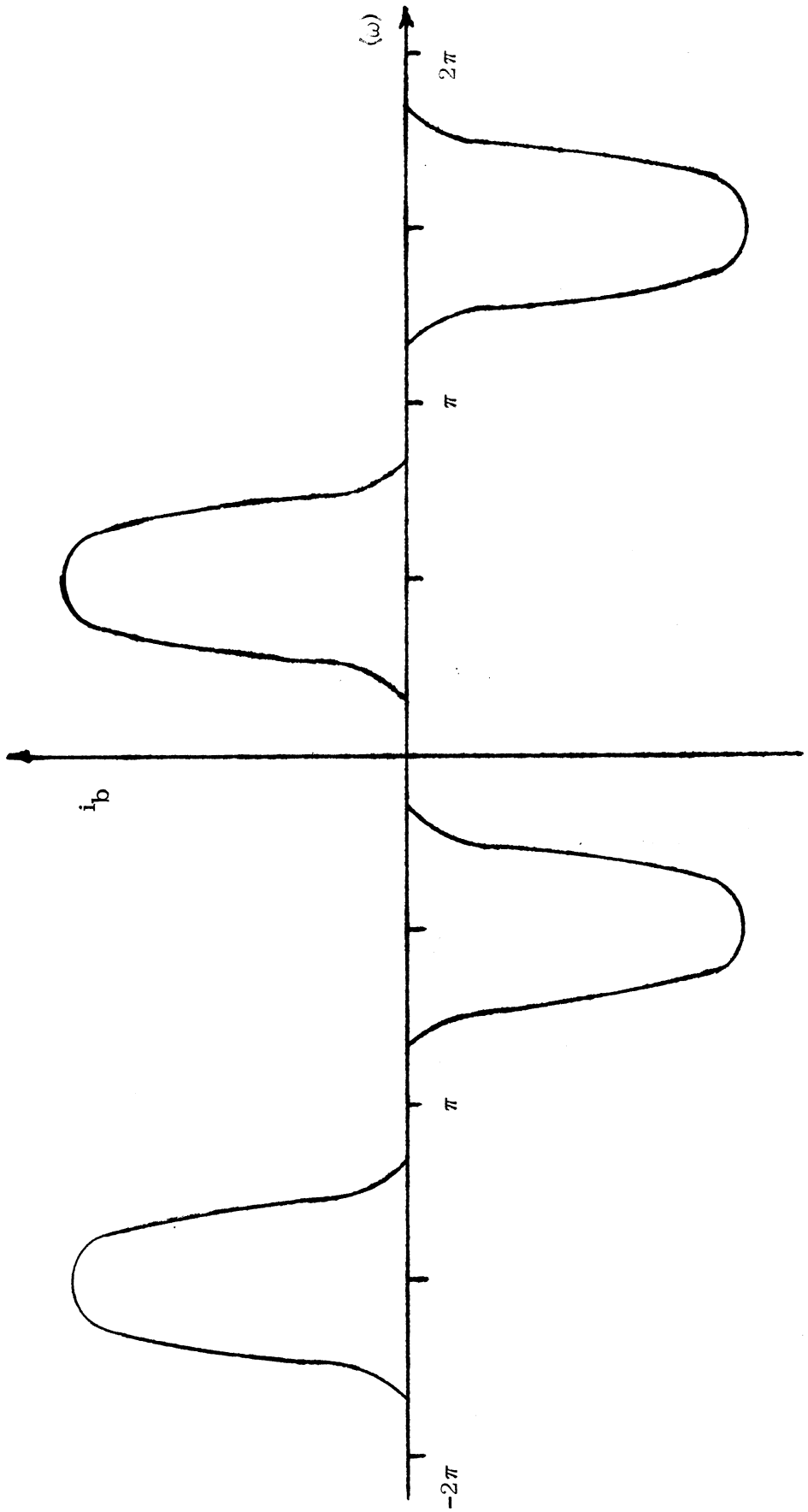

FIG. 3-4: Sketch of $i_b(t)$ for a Dual Push-Pull Tube.

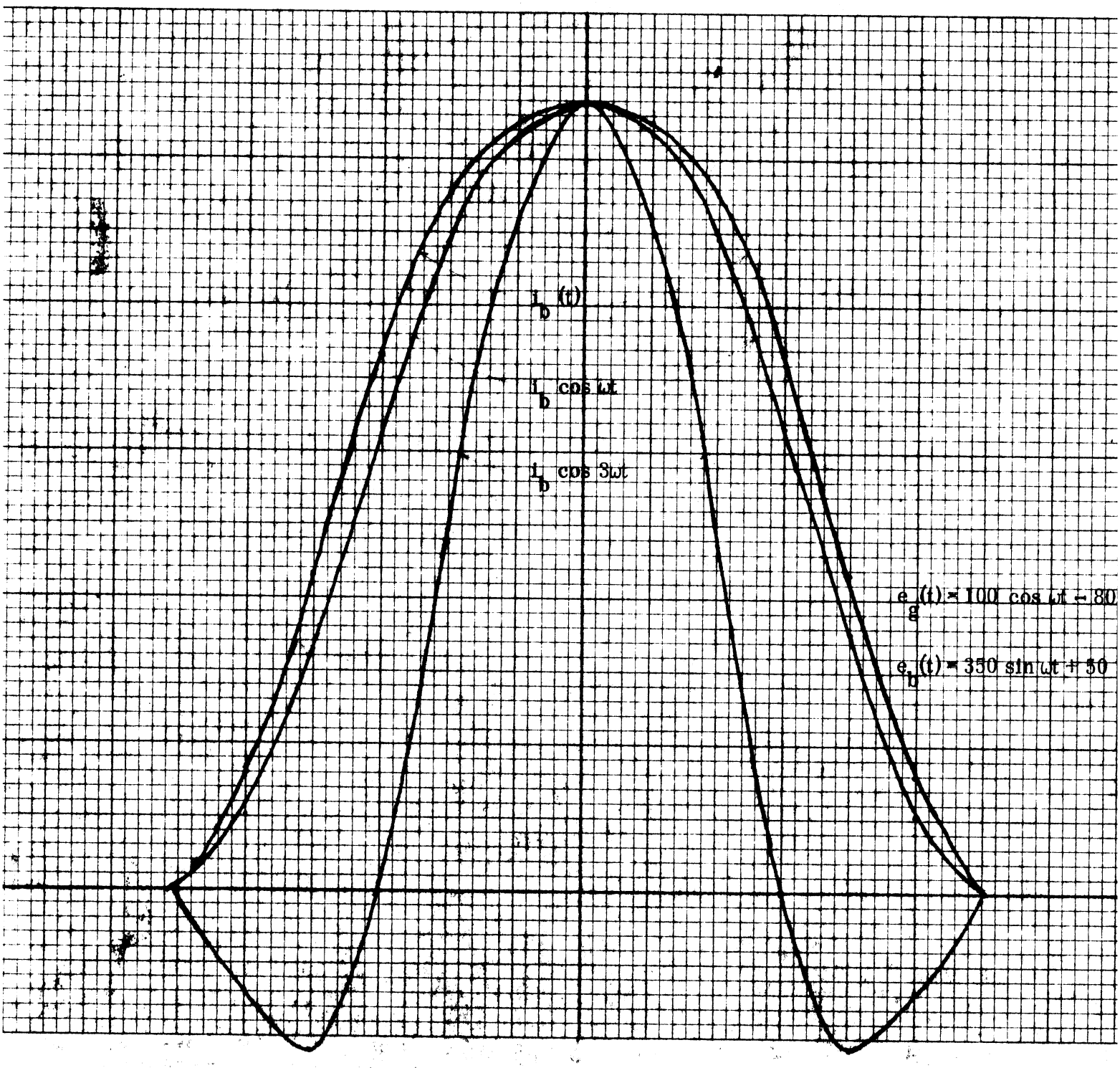

FIG. 3-5: $i_b(t)$ Calculated From Plate Curves

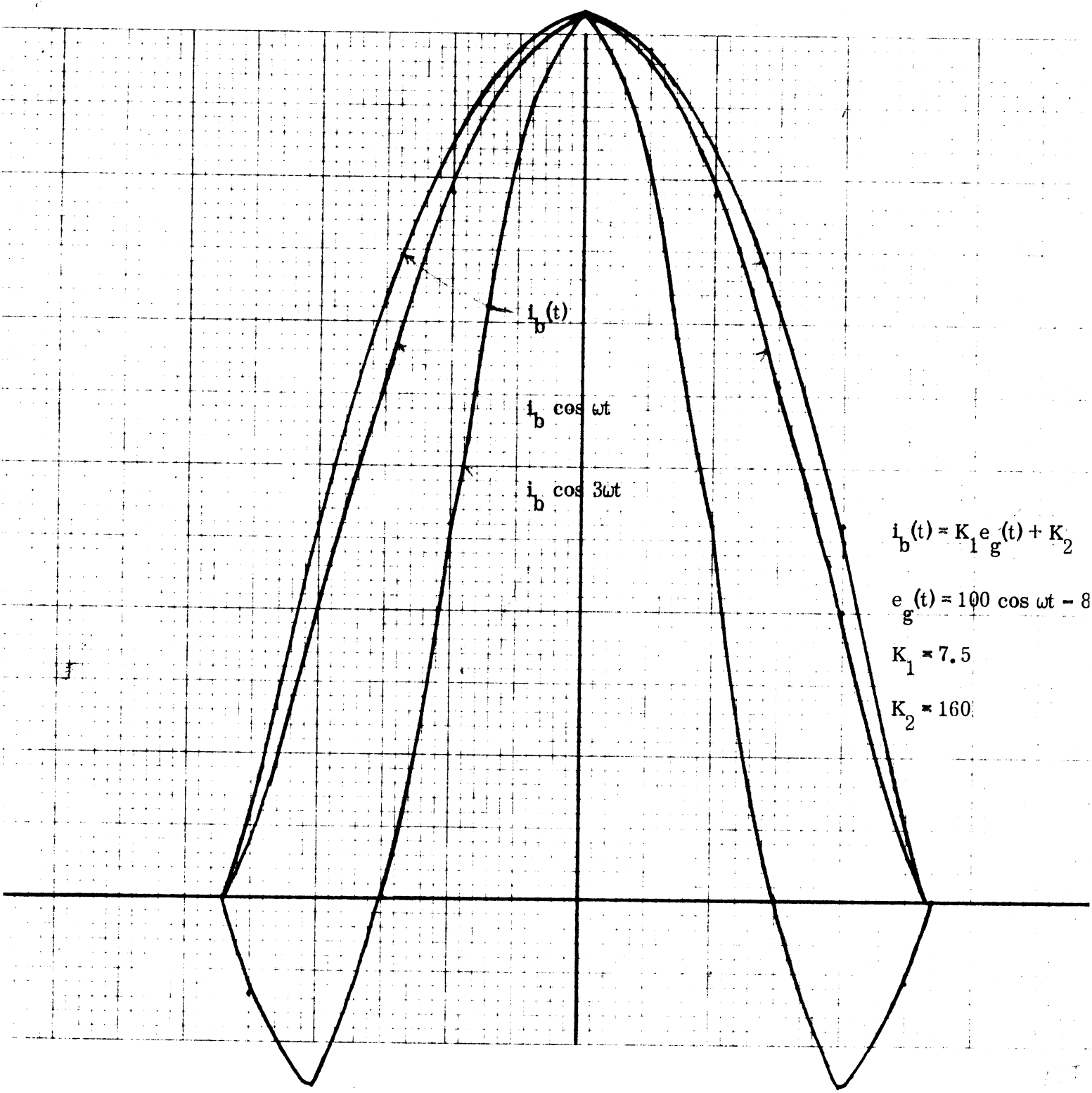

FIG. 3-6: $i_b(t)$ Calculated From Classical Model

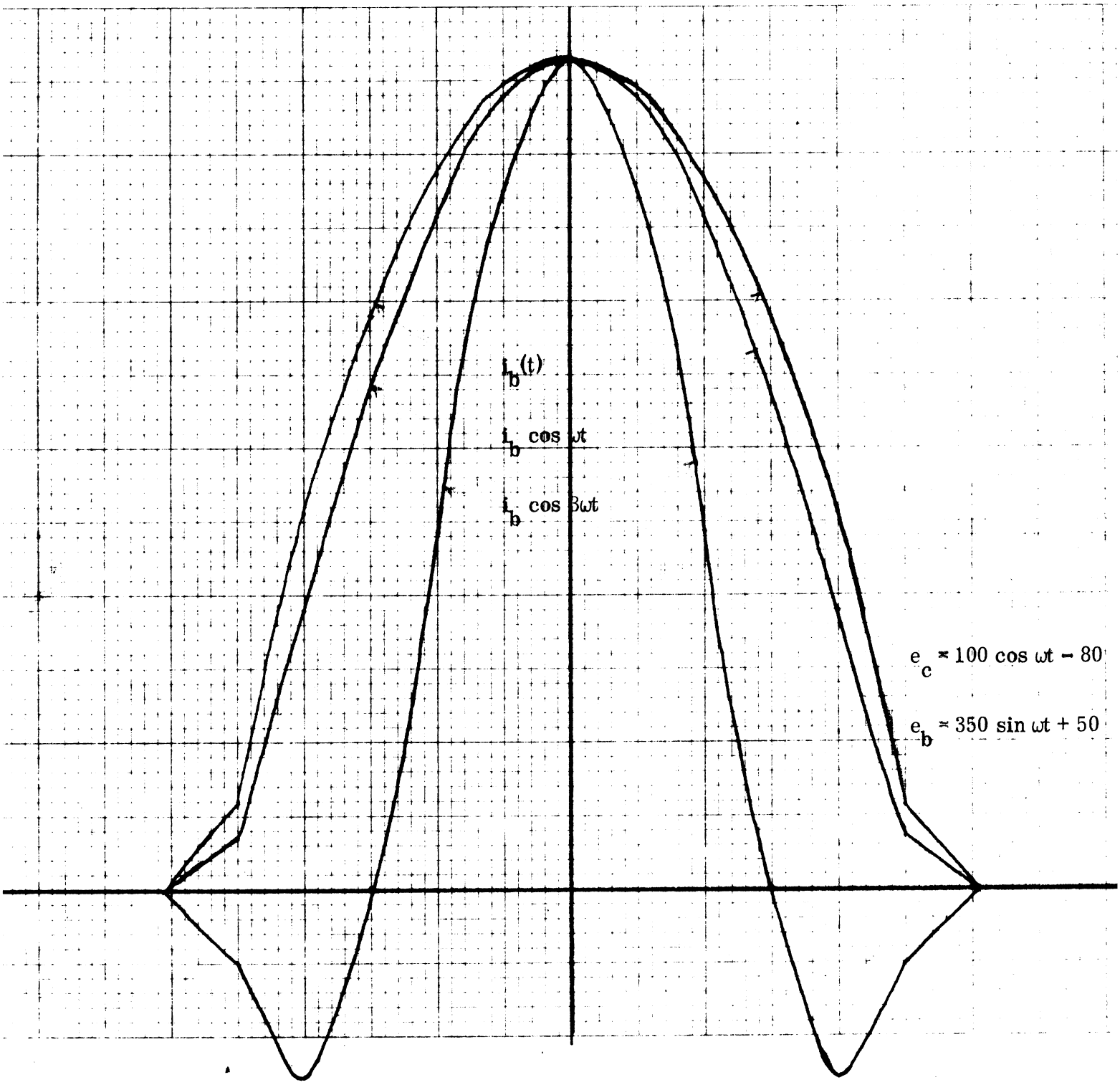

FIG. 3-7: $i_b(t)$ Calculated From Piece-Wise Linear Model No. 2.

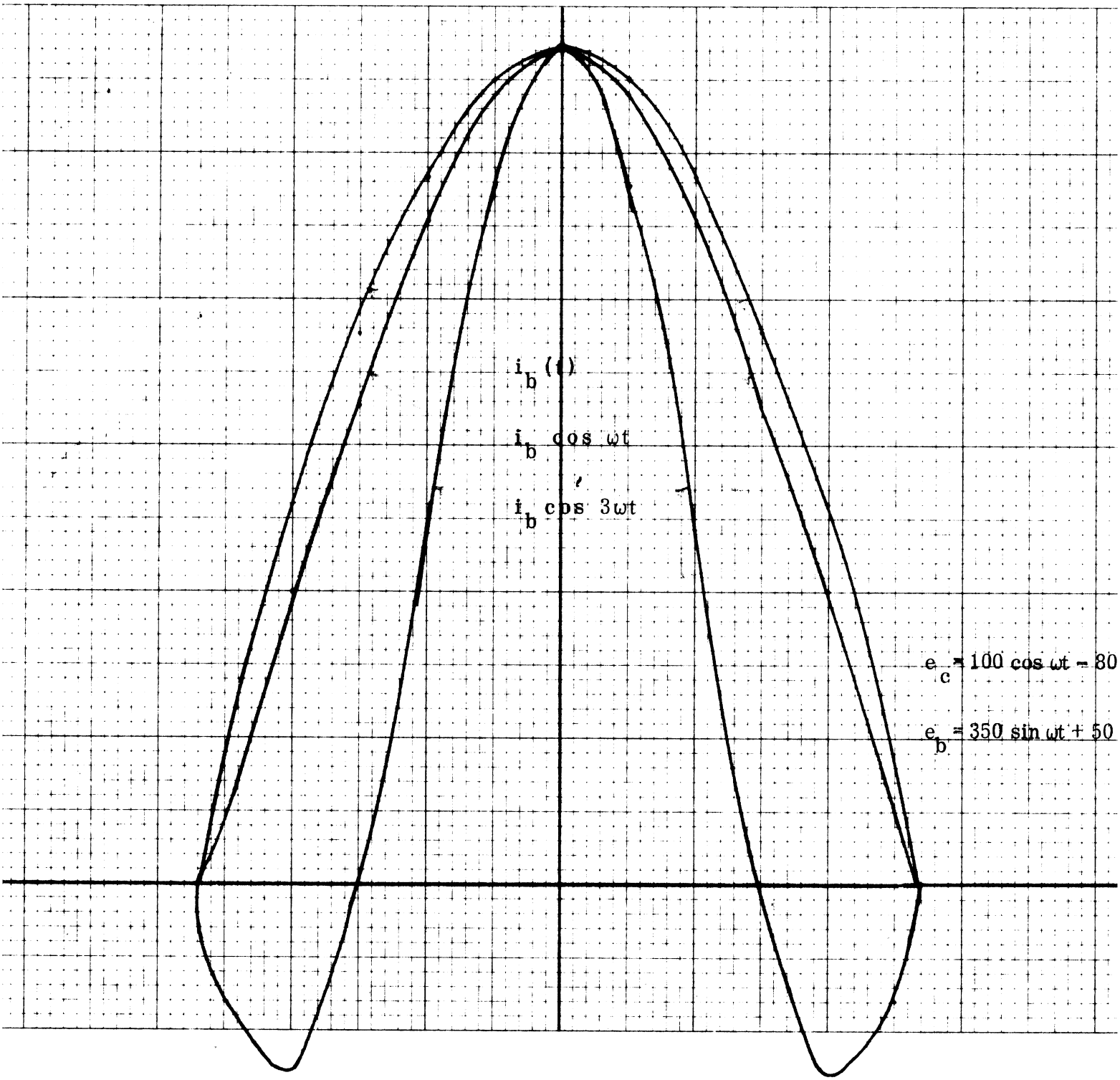

FIG. 3-8: $i_b(t)$ Calculated From Piece-Wise Linear Model No. 3.

TABLE 3-1

Three Piece-wise Linear Models

Model I

$i_b = 7.5\, e_c + 160$

Model II

$e_b < 150$

$i_b = 2\, e_c + 0.04\, e_b + 58 \qquad e_c < -15$

$i_b = 7.1\, e_c + 0.14\, e_b + 135 \qquad e_c \geq -15$

$e_b \geq 150$

$i_b = 2\, e_c + 0.013\, e_b + 58 \qquad e_c < -15$

$i_b = 7.1\, e_c + 0.048\, e_b + 135 \qquad e_c \geq -15$

Model III

$e_b < 210$	e_c	$210 \leq e_b \leq 400$
$i_b = 2.33\, e_c + .025\, e_b + 71$	$-80 \leq e_c < -19$	$i_b = 2.33\, e_c + 0.012\, e_b + 71$
$i_b = 4\, e_c + .076\, e_b + 98$	$-19 < e_c < -9$	$i_b = 4\, e_c + 0.02\, e_b + 98$
$i_b = 5.6\, e_c + 1.06\, e_b + 111$	$-9 \leq e_c < -1$	$i_b = 5.6\, e_c + 0.29\, e_b + 111$
$i_b = 7.78 + 0.148\, e_b + 123$	$-1 \leq e_c = 23$	$i_b = 7.78\, e_c + 0.04\, e_b + 123$

TABLE 3-2

Results of Model Analysis

Quant.	Tube Curves	Model 1	Model 2	Model 3
$\bar{I}_b$	109	118 (+ 7.4%)	113 (+4.1%)	114 (+4.2%)
$\lvert\bar{I}_p\rvert$ 1	199	220 (+10.5%)	207 (+ 4 %)	204 (2.5 %)
$\lvert\bar{I}_p\rvert$ 3	87.6	102 (+16.4%)	92 (+ 5 %)	85.6 (-2.5%)

appears in Fig. 3-9. Assuming that the plate voltage is a sinusoid of period ωt, the following equations apply (Cruft Laboratory, 1957).

D. C. plate input = $P_{bb} = E_{bb} I_{bb} = \bar{E}_b \bar{I}_b$ (3.12a)

Power delivered to the plate load = $P_1 = \frac{|\hat{E}_p||\hat{I}_p|}{2} = \frac{|\hat{E}_p|^2 R_1}{2}$ (3.12b)

Plate dissipation = $P_p = P_{bb} - P_1$ (3.12c)

Plate circuit efficiency = $N_p = P_1/P_{bb}$ (3.12d)

Dirving power = $P_d = \frac{1}{2} \hat{E}_g |\hat{I}_g|$ (3.12e)

Power supplied to the grid bias source = $P_{cc} = \bar{E}_{cc} \bar{I}_c$ (3.12f)

Grid dissipation = $P_g = P_d - P_{cc}$ (3.12f)

Power amplification = $A_p = P_1/P_o$ (3.12h)

All of the parameters listed above can be determined direct by the D. C. currents and voltages and A. C. voltages except P_d which includes an A. C. current. However, assuming a sinusoidial input,

$$P_d = \frac{1}{T} \int_0^T e_c i_c \, dt = \frac{1}{T} \int_0^T |\hat{E}_g| \cos \omega t \, i_c \, dt \tag{3.13}$$

If we assume that i_c flows only when $\cos \omega t = 1$,

$$P_d = \frac{|\hat{E}_g|}{T} \int_0^{T\ell} i_c \, dt = |\hat{E}_g| \bar{I}_c \tag{3.14}$$

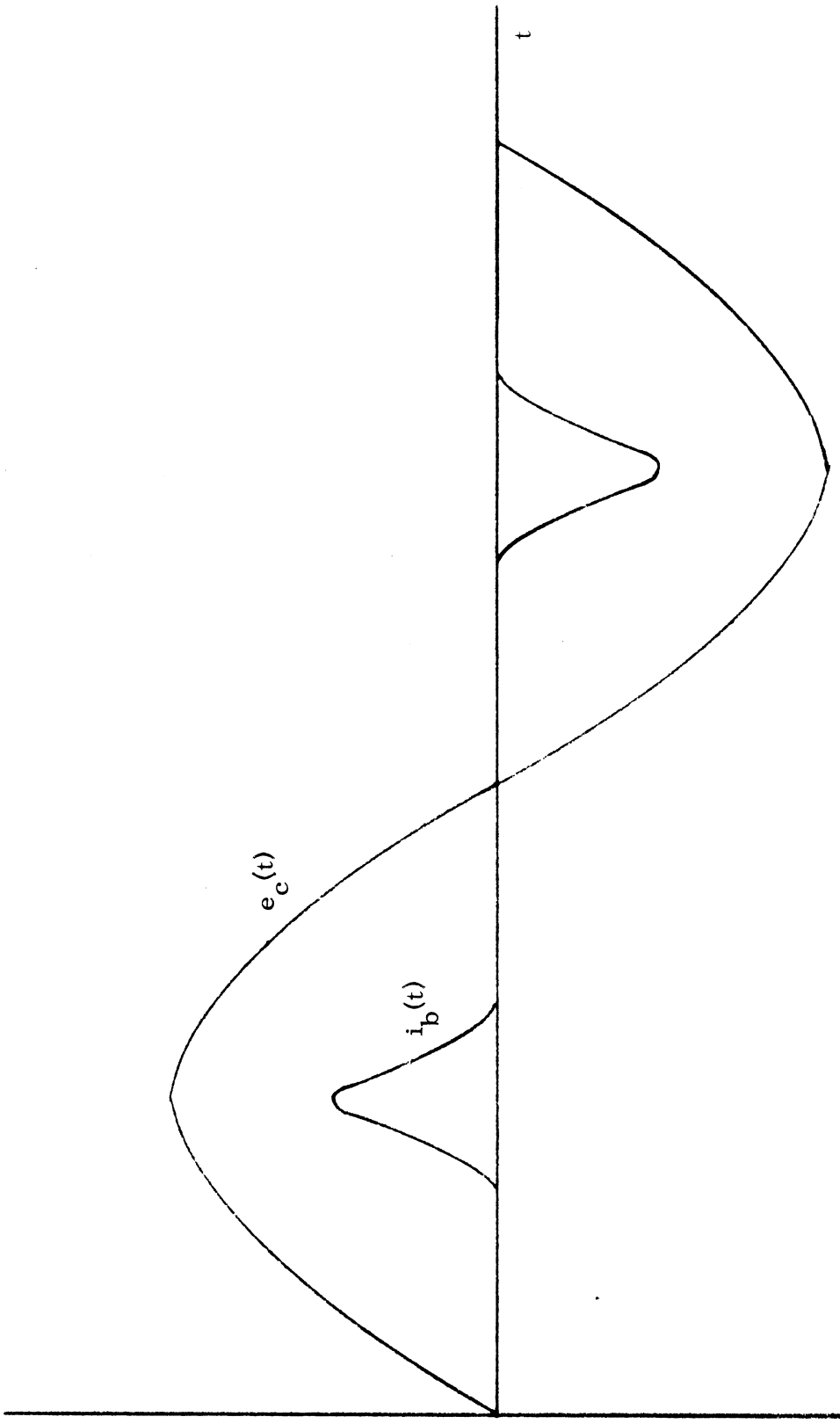

FIG. 3-9: Plate Current and Grid Voltage v.s. Time for a Push-Pull Class C Amplifier.

All of the necessary parameters are now in a form which allows them to be determined from easily measured quantities.

The selection of E_{bb}, $-E_{cc}$, $|E_g|$ and R_1 (the load impedance at the fundamental frequency) is accomplished with the aid of the tube constant current characteristics. Fig. 3-4 is the constant current characteristics of an Amperex 6252 dual tetrode. Assuming that the grid and plate voltages are sinusoids of period ωt and 180^o out of phase, the points corresponding to values of e_c and e_b for $\omega t_1 .. \omega t_2$ will form a straight line from the maximum to the minimum values of plate voltage. Let these points be Q and P respectively. The coordinates of Q are $\left[E_{bb}\right]$, $\left[-E_{cc}\right]$. Those of P are $\left[E_{bb} - \left(\hat{E}_p\right)\right]$, $\left[-E_{cc} + \hat{E}_g\right]$. The selection of Q and P (and thus E_{bb}, $|\hat{E}_p|$, $-E_{cc}$ $|E_g|$ are accomplished by a trial-and-error process as follows:

1) Select arbitrarily the points P and Q. (The tube manufacturer will usually specify normal operating supply voltages which are a good starting point).

2) Draw the line PQ.

3) Lay off from Q the following fractions of the length QP along the line: 1, 0.966, 0.866, 0.707, 0.500, and 0.259.

4) Determine, by inspection, the values of instantaneous currents at these points: i_a, i_b, i_c, ... i_f.

5) The average and fundamental components of the current are given by the formulas

$$\bar{I} = \frac{1}{12}\left[\frac{I_a}{2} + i_b + i_c + i_d + i_e + i_f\right] \tag{3.15}$$

$$(I)_1 = \frac{1}{12}\left[i_a + 1.93\, i_b + 1.73\, i_c + 1.41\, i_d + i_e + 0.52\, i_f\right] \tag{3.16}$$

$$\bar{E} = E_{bb} \tag{3.17}$$

$$(E_b)_1 = E_{bb} - e_{b\,min} \tag{3.18}$$

(The details of this analysis are given in Cruft Labs, 1957, pp. 255-259, and pp. 443-445). The constants in (3.15) and (3.16) are based on the assumption of a sinusodial excitation. Once the fundamental and D.C. components have been found, it is possible to calculate the parameters listed in (3.12a-h). The points P and Q may now be shifted and the process repeated until the desired results are obtained.

3.7 Specific Design Details

The procedure described above was used in the design of the experimental transmitter. Figure 3-10 shows three possible operating paths. The results are tabulated in Table 3-3. These values are for one (half) tube only. Path two was tentatively selected as the operating path.

3.8 Construction Details

Figures 3-11 and 3-12 are schematics of the experimental unit which was

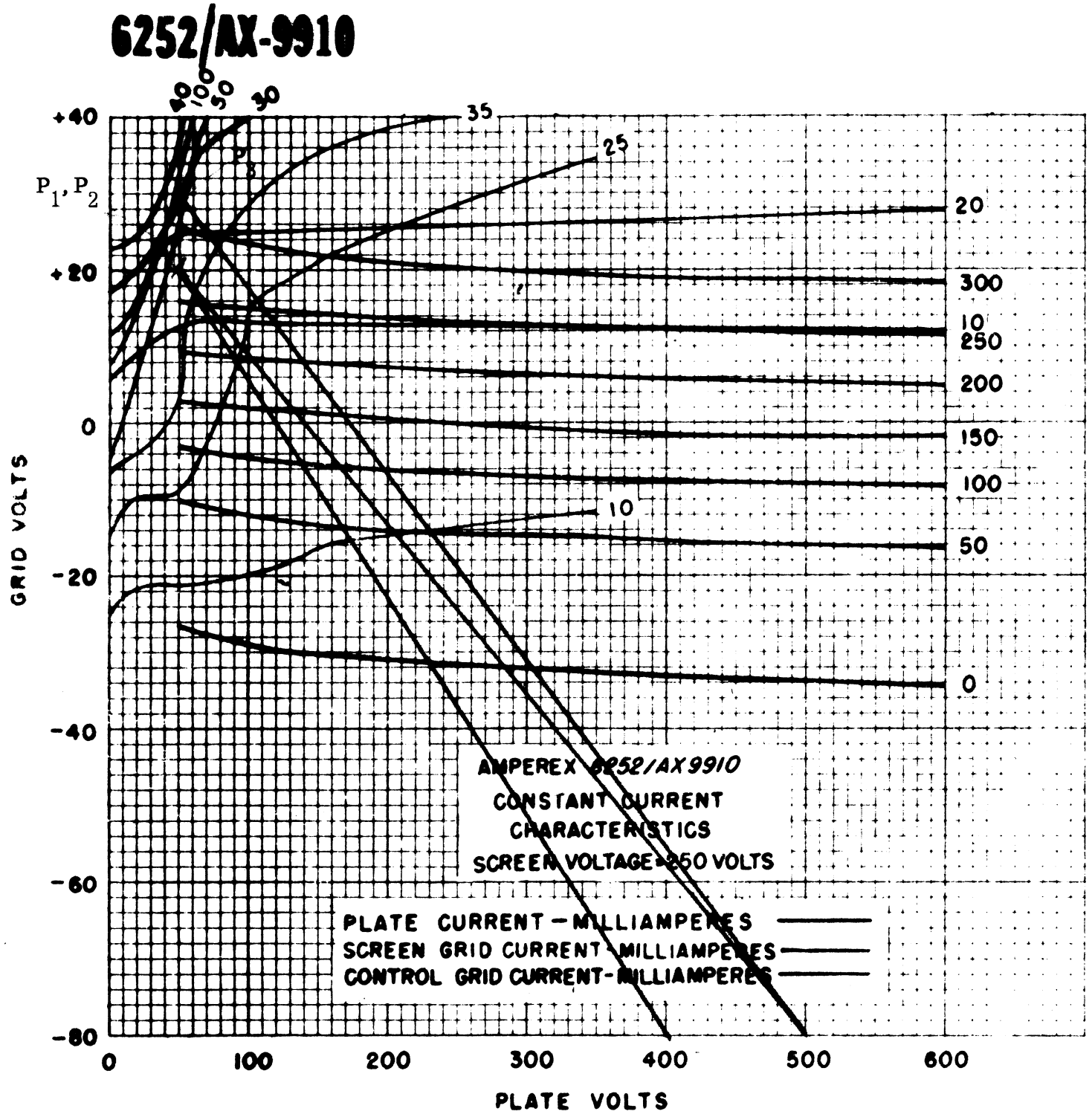

FIG. 3-10: Three Sample Operating Paths

Parameter	CCS. ABs. Max.	Path No. 1	Path No. 2	Path No. 3
I_b	68 ma (cathode)	51 ma	53.5 ma	72.3 ma
E_{bb}	500 V	500 V	400 V	500 V
$I_{p\ 1}$		98 ma	97.5 ma	128 ma
$E_{p\ 1}$		450 V	350 V	450 V
P_{bb}	30 w	27 w	21.4 w	36.2 w
P_l		22.2 w	17.1 w	28.8 w
P_p	6.7 w	4.8 w	4.3 w	7.4 w
N_p		82 per cent	80 per cent	80 per cent
P_l		4500 Ω	3600 Ω	3500 Ω
Screen	300 V	250 V	250 V	250 V
I_c	2 ma	2.4 ma	2 ma	4.25 ma
E_{cc}	- 200 V	-80 V	-80 V	-80 V
$I_{g\ 1}$		4.2 ma	3.9 ma	
$E_{g\ 1}$		100 V	100 V	110 V
P_{cc}	.5 w	0.2 w	0.16 w	
P_g		0.04 w	0.04 w	
P_d		0.24 w	0.2 w	4.68 w
A_p		92.5	85.5	

TABLE 3-3

Results from the Three Paths Shown in Fig. 3-10.

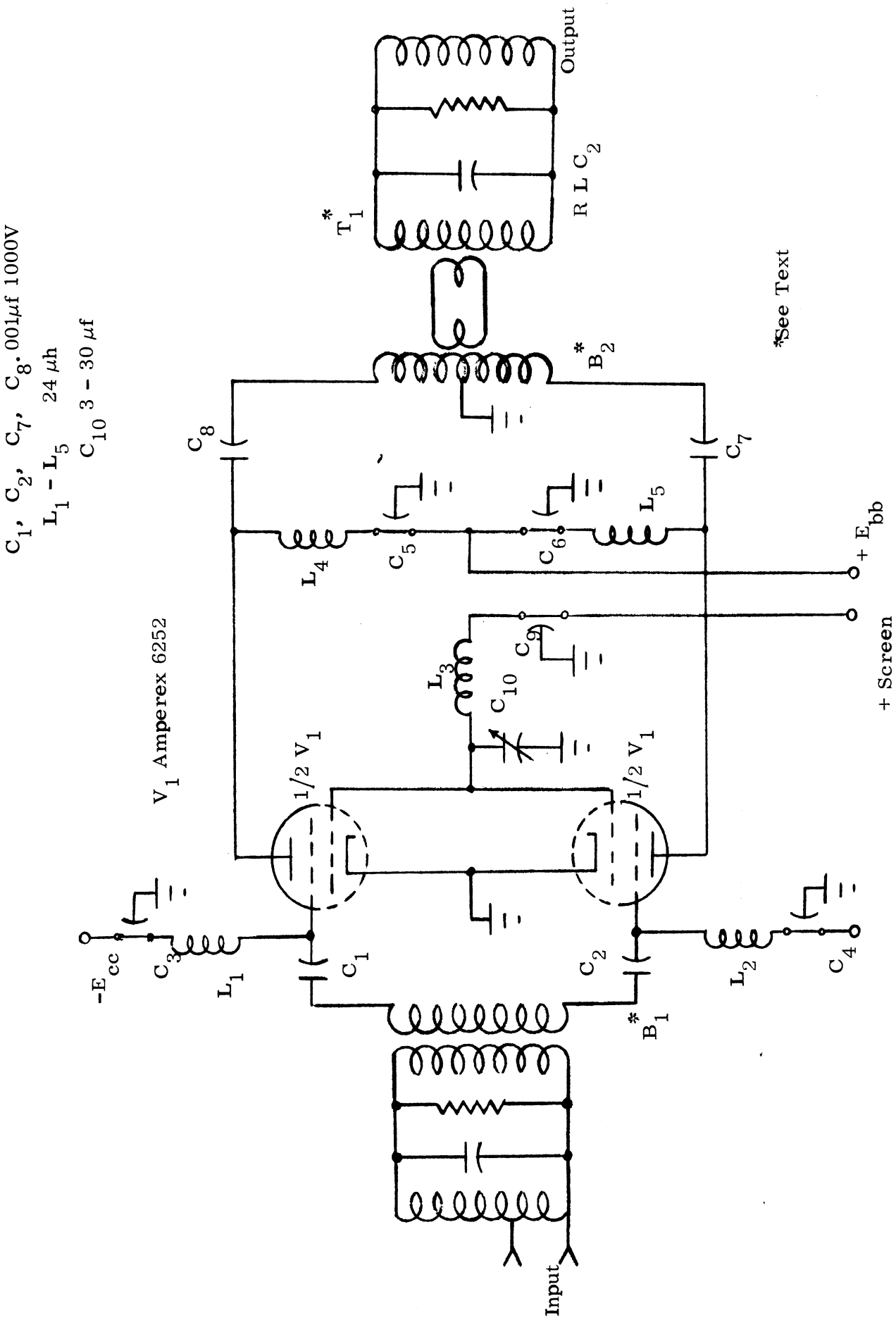

FIG. 3-11: Schematic of Experimental Amplifier

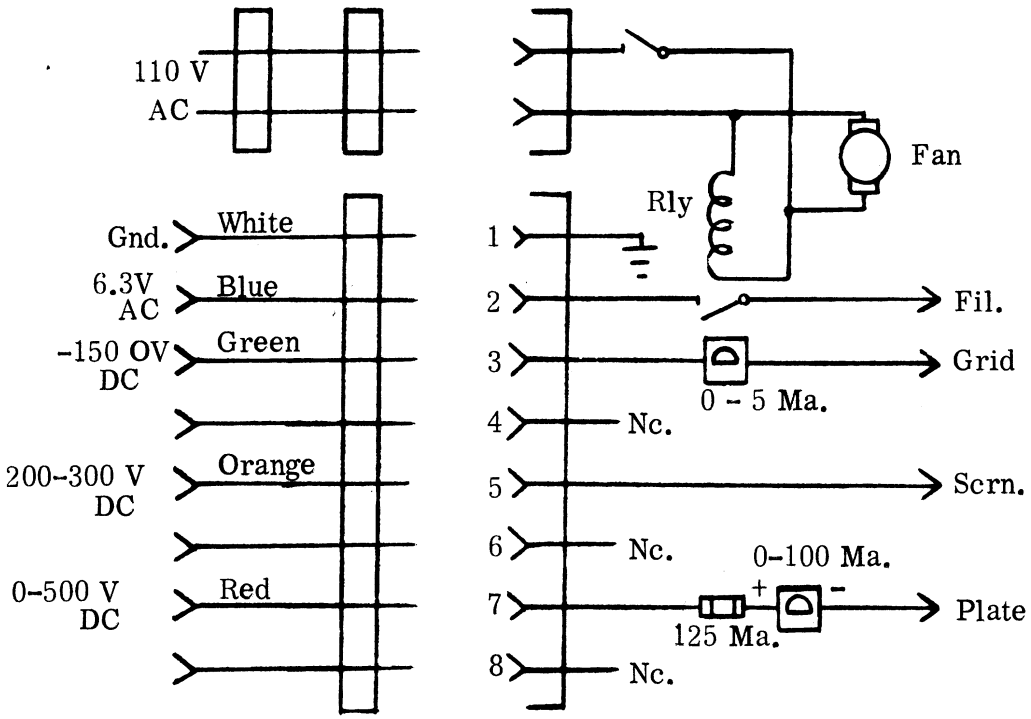

FIG. 3-12: D. C. Meters and Cables for Experimental Amplifier

constructed. The layout of the R. F. section is shown in Fig. 3-13 and a sketch of the complete unit in Fig. 3-14. The construction is quite typical except for the use of coaxial tuned circuits. The baluns are 15" broadband coaxial baluns (Duncan and Minerva, 1960). The transformer T, is a quarter wave transformer with an impedance transformation ratio of 10:1 and the tune circuits are shorted lengths of coaxial transmission line. It is well known that resonant circuits composed of lumped circuit elements can be constructed for use at 300 MHz. However, the primary purpose of this study is to evaluate transmitter performance at the harmonics of 300 MHz as a function of the circuit parameters. The behavior of conventional coils and capacitors is not well understood at microwave frequencies.

The design of the output circuitry was accomplished in the following manner. Knowing that an impedance of $R = 3600\Omega$ at the fundamental frequency was necessary at each plate of the 6252 in order to provide operation along path 2 described above, the impedance transfer function of the balun was measured using a slotted line and a known balanced load.

$T_{balun} = Z_{unbal.} / Z_{bal} = (0.18 + j0.35)$, thus in order to see $Z_b = R = 3600$, Z_u must equal (648 + j 1260) which is $Z_u / Z_o = 13 + j25.2$ or a VSWR of $\simeq 62$. A sketch of the tank circuit appears in Fig. 3-14. Choosing a design Q of about 10 and recalling $Q = W C I R$ where $C = 1.78 \mu\mu r/$ in for 50 Ω air line $\ell \simeq \lambda/4_{300} \simeq 10"$ R must be $\simeq 300\ \Omega$. Referring to Fig. 3-15, the admittance of a short circuit is located at point A. Transforming this through 1, adding the load ($Y = 1.0 + j0$)

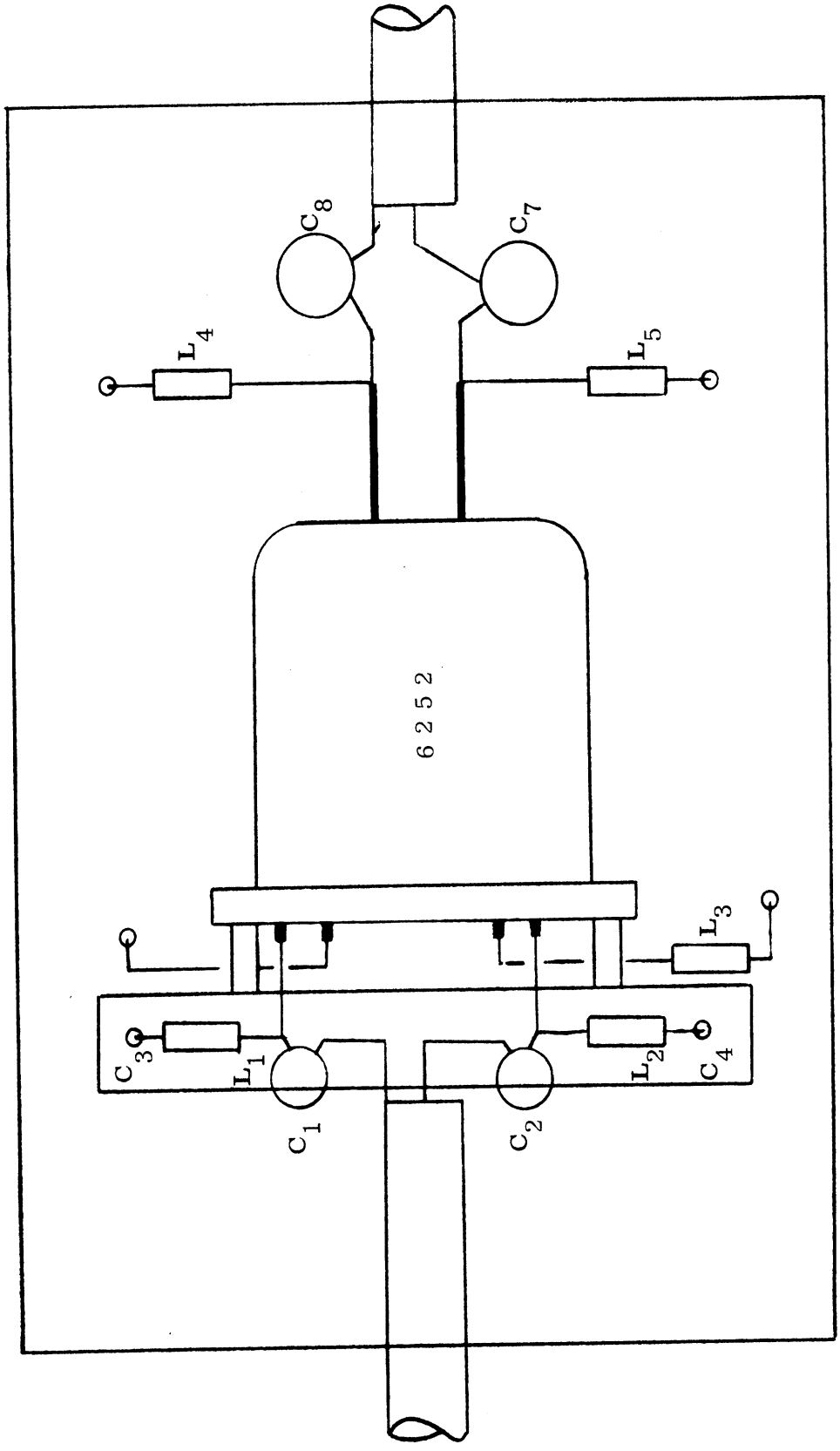

FIG. 3-13: Amplifier Lay-Out Details

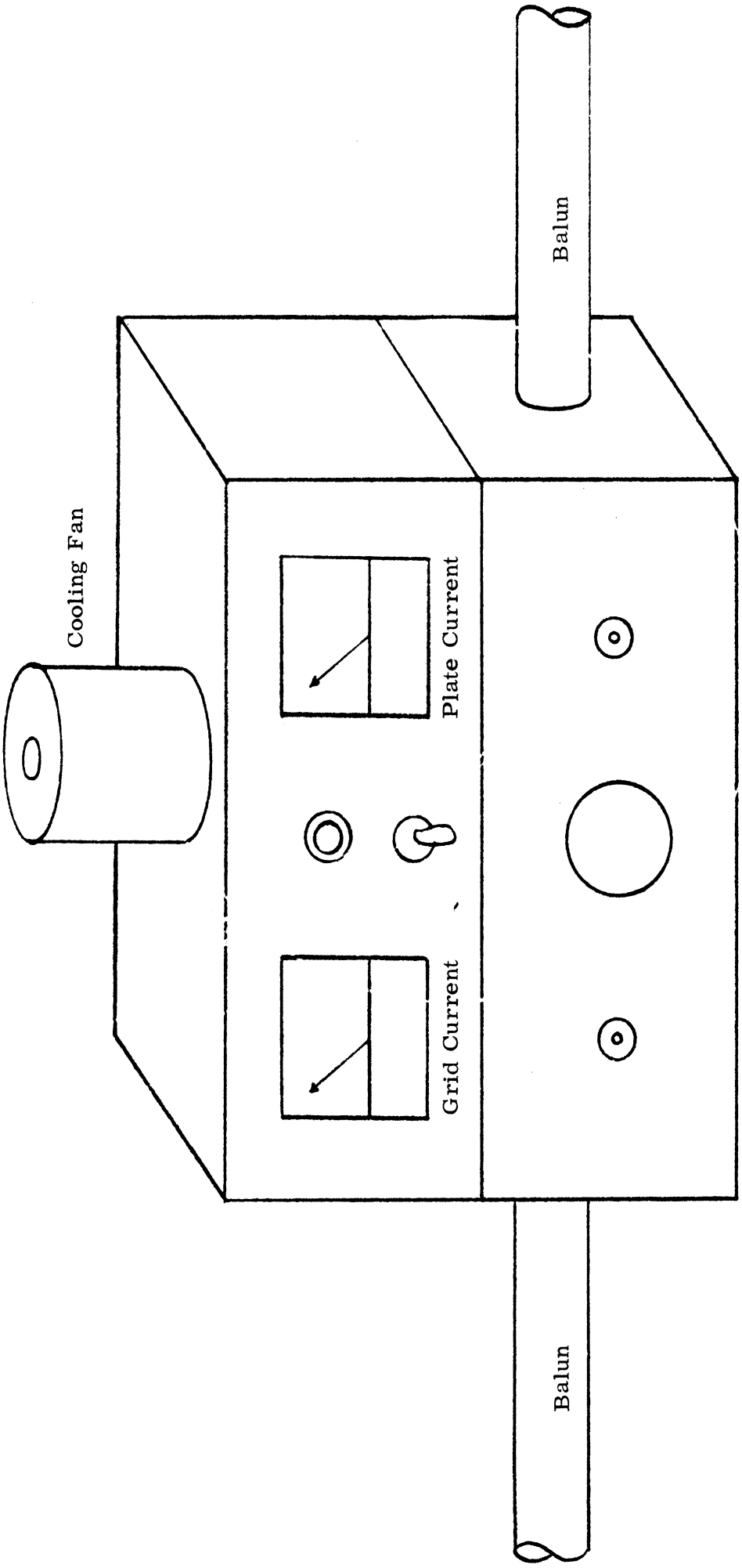

FIG. 3-14: Sketch of the Completed Transmitter

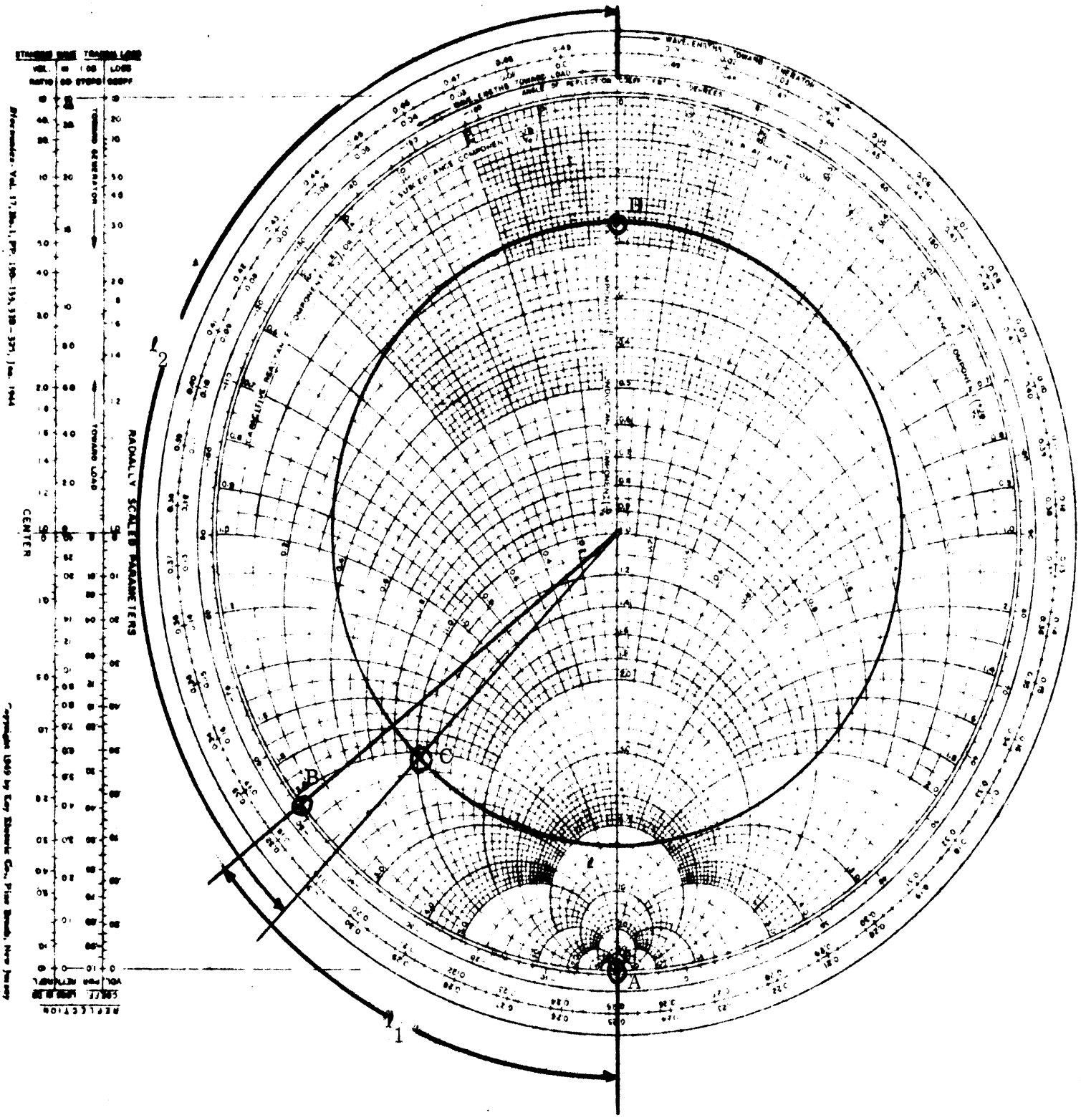

FIG. 3-15: Design of the Resonant Output Circuit

and transforming through ℓ_2 we have that $\ell_1 = 2.88''$, $\ell_2 = 7.40''$. It is now necessary to transform the $R/Z_o = 6$ seen at the end of the tuned circuit to the Z/Z_o $13 + j25.2$ needed at the balun. A two section quarter wave transformer was constructed as follows. The impedance transformation afforded by each section is given by

$$Z_{in}\, Z_{out} = Z_o \tag{3.19}$$

Thus for two sections in series,

$$Z_{01} = Z_1 Z_2 \qquad Z_{02} = Z_2 Z_3 \tag{3.20}$$

or

$$Z_3/Z_1 = Z_{02}^2/Z_{01}^2$$

Since we need a $Z_3/Z_1 = 10$,

$$Z_{02}/Z_{01} = \sqrt{10} = 3.36.$$

The values selected were $Z_{01} = 35\ \Omega$, $Z_{02} = 125\Omega$

The input resonant circuit was constructed similar to the output, and the transmitter was excited by an ARC-27. The output spectrum measurement scheme is given in Fig. 3-16.

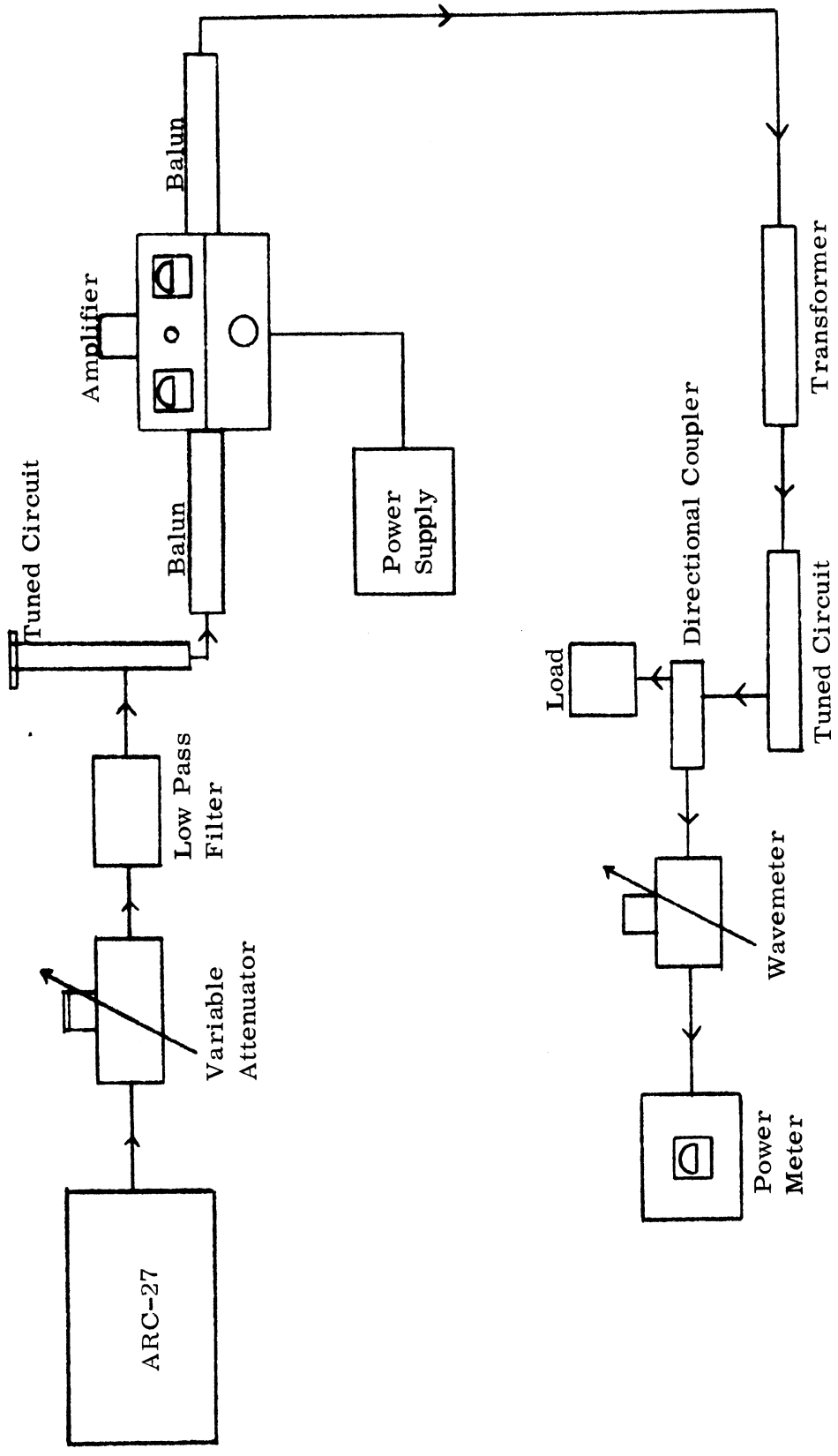

FIG. 3-16: Schematic of Spectrum Signature Measurement Test

IV. EXPERIMENTAL INVESTIGATION OF TRANSMITTER NON-LINEARITIES

During this portion of the investigation, consideration has been given to load impedance variations at the fundamental frequency and their effects on the power output at the harmonic frequencies. During this investigation both ARC-27 and ARC-34 transmitters have been evaluated.

Typical harmonic Rieke diagrams are shown in Figs. 4-1 and 4-2. These diagrams were measured employing the test setup shown in Fig. 4-3. It is apparent from the harmonic Rieke diagram of Fig. 4-1 that the transmitter is not pseudo-linear, e.g., power variations are greater than 3db. This unit was an ARC-27 that was not properly tuned and as a consequence this may have contributed to the non-linear effects. This supposition is further substantiated from the data that is presented in Fig. 4-2 where the power variations are less than 3db such that the unit has been designated as pseudo-linear. It will be observed that the power level recorded was measured at the second harmonic frequency (600 MHz.) as a function of the load impedance at the fundamental frequency (300 MHz). The data was collected by terminating the transmitter in a matched load with respect to the transmission line at 600 MHz and a mis-match (VSWR's of 1.2, 1.5, 2.0, 3.0, and 5.0) at 300 MHz. The power level was monitored at the harmonic frequency as the load impedance angle at the fundamental frequency was varied through 180^{o}.

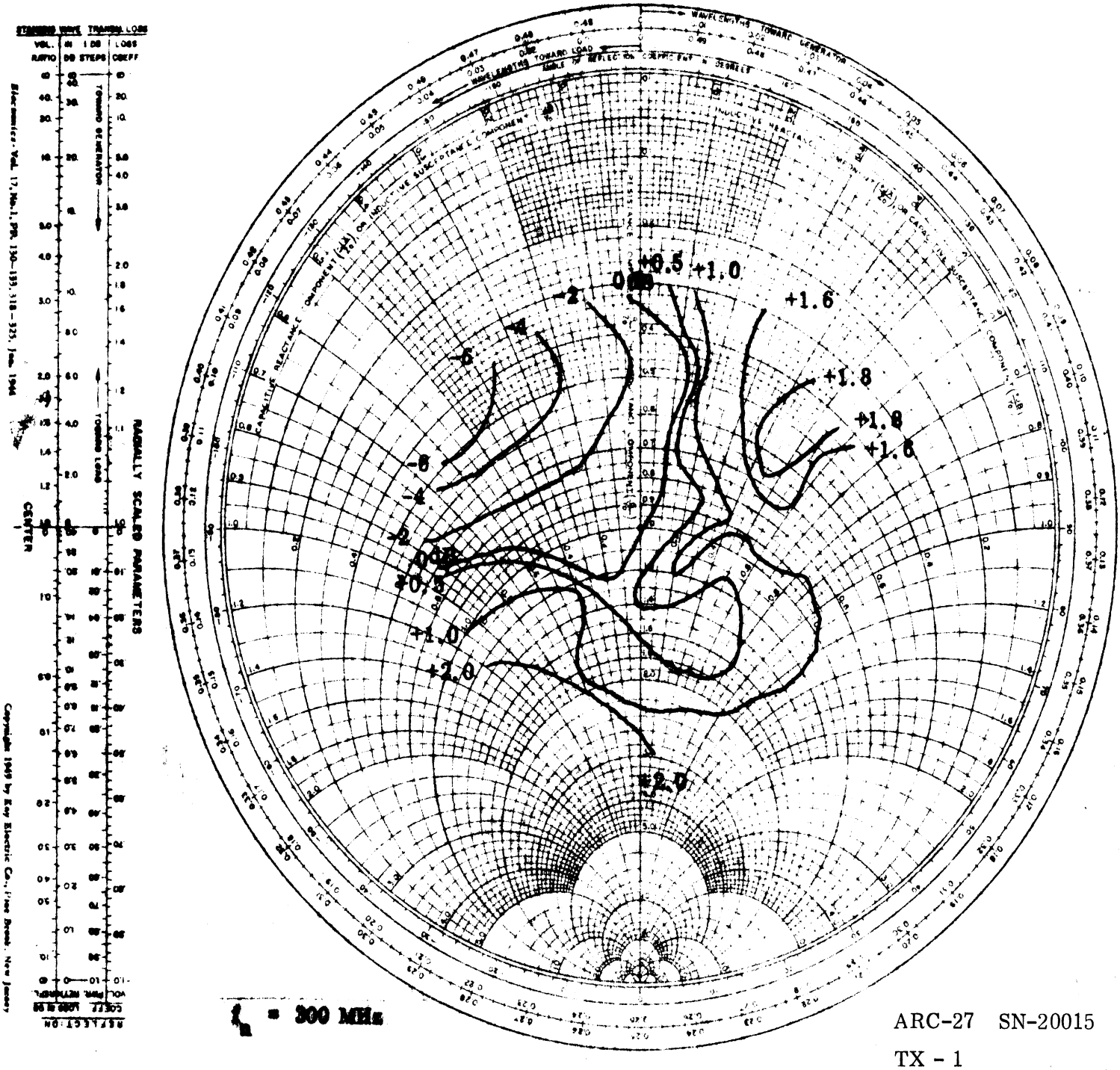

FIG. 4-1: Harmonic Rieke Diagram for SN-20015

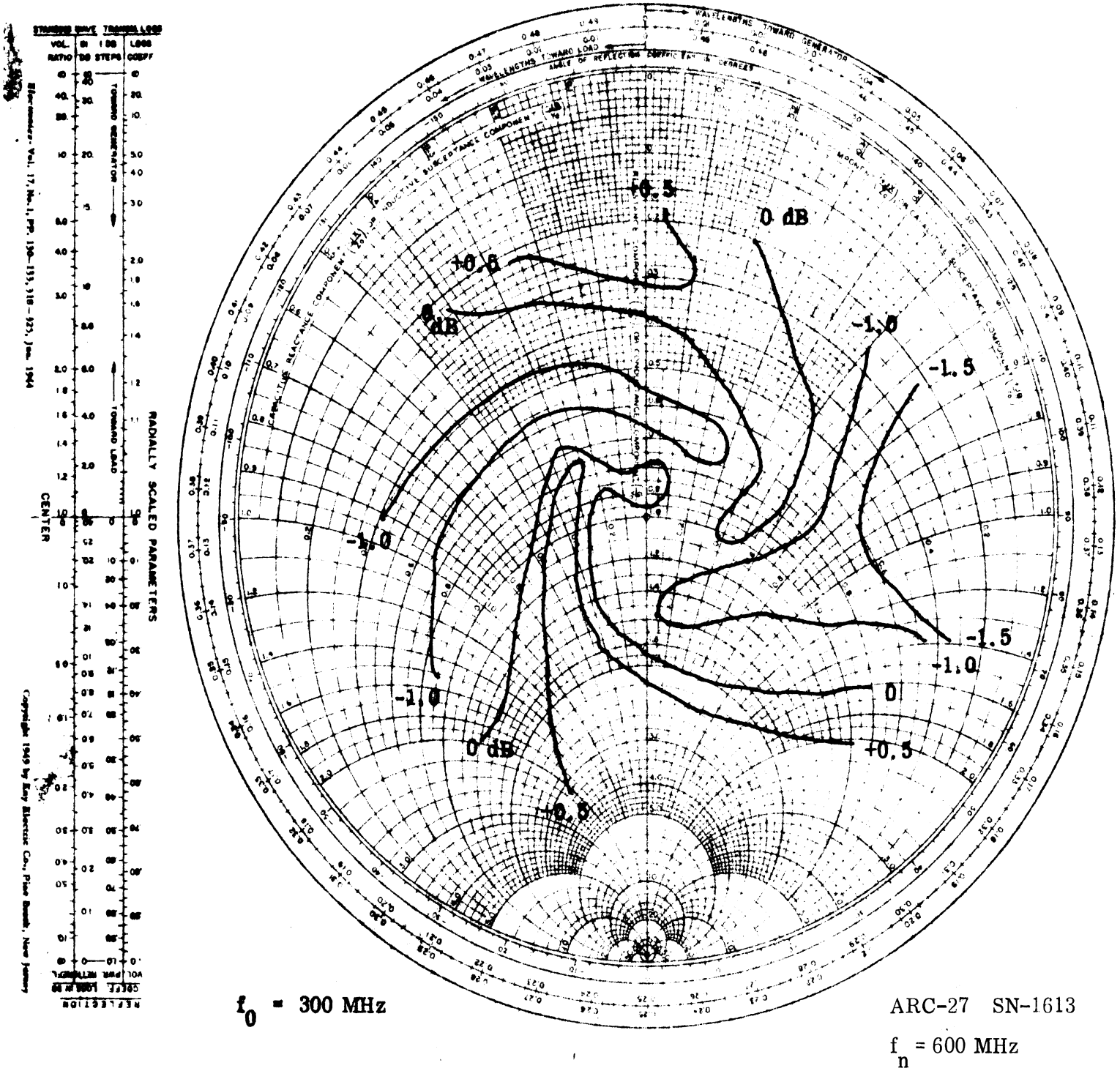

FIG. 4-2: Harmonic Rieke Diagram for SN-1613

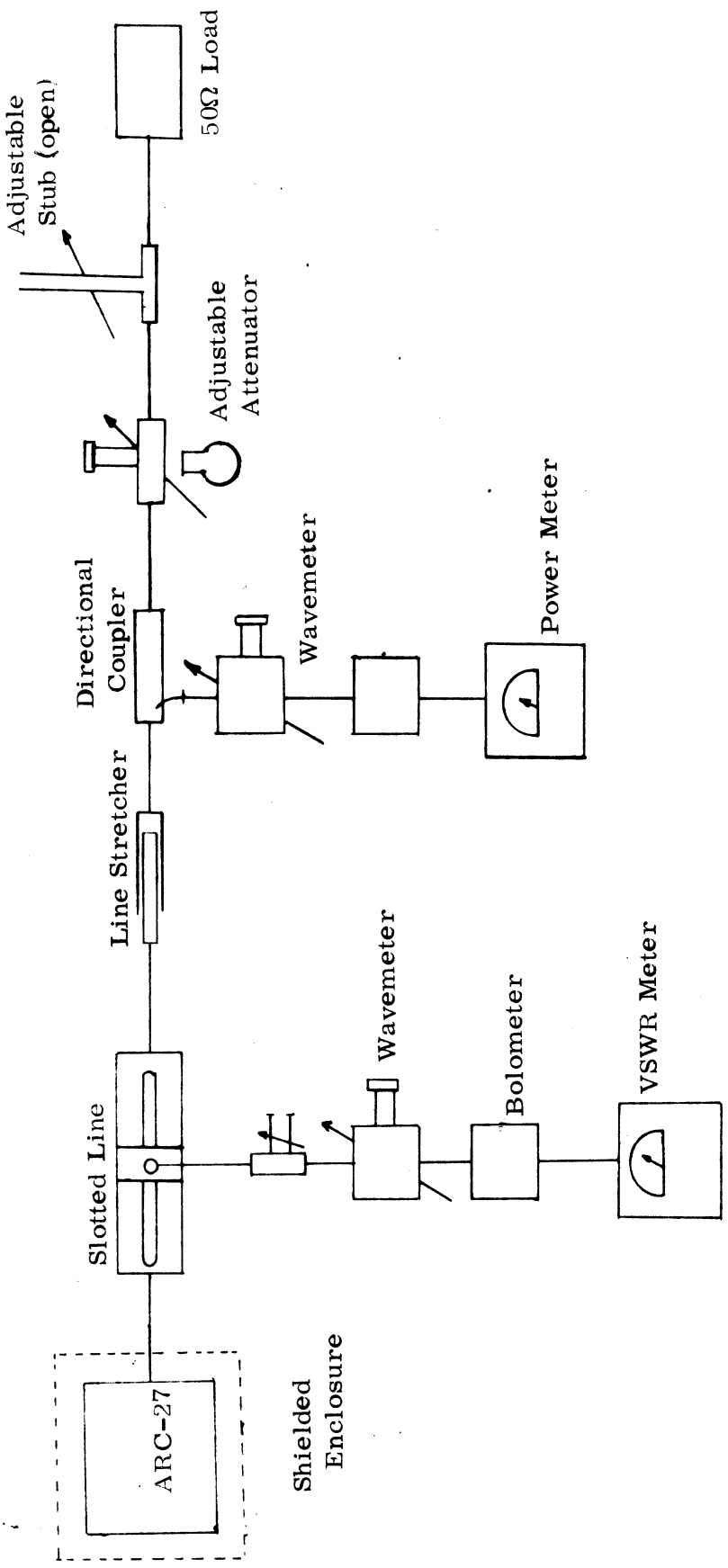

FIG. 4-3: Experimental "Harmonic Rieke Diagram" Equipment Arrangement

Additional harmonic Rieke diagrams have been collected for two ARC-34 transmitters, however, contour plots have not been plotted. It has been observed that in general it is not appropriate for the ARC-34 to be termed a pseudo-linear device.

Power transfer data has been collected for a constant VSWR load at the fundamental frequency with the load varying at the harmonics; this has not yet been plotted. The data appears to be in good agreement with the theoretical curves that have been presented in previous reports (Ferris, et al, 1967).

V. CONCLUSIONS

The class C amplifier has recently been completed and the sole experimental result is, that given bias voltages and an input signal, there exists an output.

Similarly, the transmitter analytical model has only been solved for sinusodial inputs and outputs. One interesting result not included here was the selection of a load with a reactive component providing a relative phase shift between the input and output voltages. A graphical analysis was done for such a case using a phase shift of 10^{o}. The results showed no appreciable change in the waveform of i_b from that given in Fig. 3-5.

A more realistic model would, of course, include the tube input, output, and plate grid coupling capacitances. In addition, the 6252 has a neutralizing capacitance from the grid of unit 1 to the plate of unit 2 and vice versa. This must also be included in a detailed analysis.

With the experimental data obtained to date and the analysis that has been accomplished, it is not yet possible to say to what extent the characteristics of either the ARC-27 or the ARC-24 can be determined by linear prediction techniques.

APPENDIX

i_b total instantaneous plate current

$\bar{I}_b$ average (DC) plate current

$\hat{I}_{p|n}$ magnitude of the n'th component of plate current

e_b total instantaneous plate voltage

$\bar{E}_b$ average (DC) plate voltage

$\bar{E}_{bb}$ plate supply voltage

$|\hat{E}_{p|n}|$ magnitude of the n'th component of plate voltage

e_c total instantaneous grid voltage

$\bar{E}_c$ average (DC) grid voltage

$\bar{E}_{cc}$ grid supply voltage

$|\hat{E}_{g|n}|$ magnitude of the n'th component of grid voltage

i_c total instantaneous grid current

$\bar{I}_c$ average (DC) grid current

$|\hat{I}_{g|n}|$ magnitude of the n'th component of grid voltage

P_{bb} DC plate input power

P_l power delivered to the plate load

P_p plate dissipation

N_p plate circuit efficiency

P_d input driving power

P_g grid dissipation

P_{cc} power supplied to the grid bias source

A_p power amplification

REFERENCES

Cheng, David K. Analysis of Linear Systems, Addison-Wesley, Reading, Mass., 1959, Chapter V.

Cruft Laboratory, Electronic Circuits and Tubes, McGraw-Hill, New York, N.Y., 1947, pp. 423-462.

Duncan, J.W. and V.P. Minerva, "100:1 Bandwidth Balun Transformer", Proc. IRE, Vol. 48, No. 2, February, 1960, pp. 156-164.

Ferris, J.E., W.R. DeHart and W.B. Henry, "Transmitter Impedance Characteristics for Airborne Spectrum Signature", Interim Technical Report No. 3, January, 1967, University of Michigan Radiation Laboratory Report 7956-3-T, 14 pages.

Skilling, H.H., Electrical Engineering Circuits, John Wiley and Sons, New York, N.Y., 1957, pp. 439-442.